

Generalized Multi-hop Pressure for Heterogeneous Perimeter Control

Xiaocan Li

Department of Mechanical and Industrial Engineering
University of Toronto, Toronto, Canada
Email: hsiaotsan.li@mail.utoronto.ca

Xiaoyu Wang

Department of Civil and Mineral Engineering
University of Toronto, Toronto, Canada
Email: cnxiaoyu.wang@mail.utoronto.ca

Ilia Smirnov

Department of Civil and Mineral Engineering
University of Toronto, Toronto, Canada
Email: ilia.smirnov@utoronto.ca

Scott Sanner

Department of Mechanical and Industrial Engineering
University of Toronto, Toronto, Canada
Email: ssanner@mie.utoronto.ca

Baher Abdulhai

Department of Civil and Mineral Engineering
University of Toronto, Toronto, Canada
Email: baher.abdulhai@utoronto.ca

Abstract

Perimeter control prevents loss of traffic network capacity due to congestion in urban areas. Homogeneous perimeter control allows all access points to a protected region to have the same maximal permitted inflow. However, homogeneous perimeter control performs poorly when the congestion in the protected region is heterogeneous (e.g., imbalanced demand) since the homogeneous perimeter control does not consider location-specific traffic conditions around the perimeter.

When the protected region has spatially heterogeneous congestion, it can often make sense to modulate the perimeter inflow rate to be higher near low-density regions and vice versa for high-density regions. To assist with this modulation, we can leverage the concept of 1-hop traffic pressure to measure intersection-level traffic congestion. However, as we show, 1-hop pressure turns out to be too spatially myopic for perimeter control and hence we formulate multi-hop generalizations of pressure that look “deeper” inside the perimeter beyond the entry intersection. In addition, we formulate a simple heterogeneous perimeter control methodology that can leverage this novel multi-hop pressure to redistribute the total permitted inflow provided by the homogeneous perimeter controller. Experimental results show that our heterogeneous perimeter control policies leveraging multi-hop pressure significantly outperform homogeneous perimeter control in scenarios where the origin-destination flows are highly imbalanced with high spatial heterogeneity.

INTRODUCTION

Perimeter control regulates transfer flows among protected regions by limiting the permitted inflow for the feeder links of protected regions, ensuring that each protected region’s vehicle accumulation does not exceed a critical value that would negatively impact traffic productivity in protected regions. Perimeter control usually relies on Macroscopic Fundamental Diagrams (MFDs), which describe the relationship between traffic productivity and congestion levels and are widely used in numerous studies [1, 2, 3]. For MFD-based perimeter control, control parameters design relies on the function of MFDs and critical value of vehicle accumulation [4, 5, 6]. However, the accuracy of MFDs is severely affected by their strong assumption of the homogeneity of congestion distribution within each region. Lower homogeneity (higher heterogeneity) results in lower accuracy of MFDs [7], and consequently adversely affects the performance of MFD-based perimeter controllers.

As a concrete example of the limitations of the homogeneity assumption of MFDs, we refer to Figure 1a, where we see an example of an inner region with internally imbalanced congestion. In this case, choosing a homogeneous rate of inflow around the perimeter boundary may oversaturate the upper region while under-utilizing traffic capacity in the lower region.

In contrast to MFDs that model aggregated congestion metrics at the region and network level, there is also a class of metrics aiming to measure congestion at the local intersection level. Specifically, the notion of 1-hop traffic pressure quantifies the traffic difference between an upstream link and its immediate downstream links, which is inspired by related work in communication networks [8, 9, 10]. Formally, the mathematical definition of 1-hop pressure is in Eq. (1), where $S(l)$ is a traffic statistic (such as queue density, flow) for link l , $\mathcal{N}(l, 1)$ is the set of 1-hop downstream links for link l , and T_{lj} is the turning ratio from link l to j :

$$p(l, 1) = S(l) - \sum_{j \in \mathcal{N}(l, 1)} T_{lj} S(j) \quad (1)$$

From the perspective of 1-hop pressure, we can instead analyze an intersection-level view of congestion in Figure 1b. Here, we see that the pressure at each perimeter boundary intersection provides a local indication of where to provide perimeter inflow to minimize congestion. In this case, the intersections at the lower region boundary (e.g., feeder link B) have higher pressure than the upper region (e.g., feeder link A), making it more sensible to permit larger inflows in the lower region.

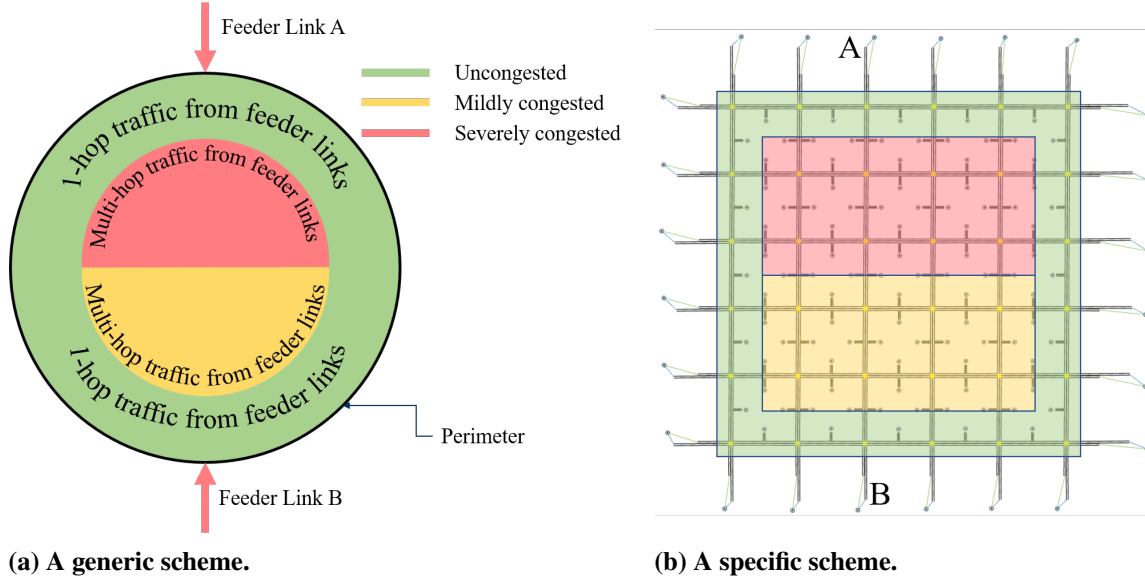


Figure 1 A generic and specific scheme showing why 1-hop pressure is myopic for perimeter control and the need for multi-hop pressure.

While modulating perimeter inflow according to 1-hop pressure seems to provide a clear solution to the drawbacks of MFD-based homogeneous perimeter control as described above, the existing 1-hop pressure fails to differentiate feeder link A and B, and therefore cannot improve the performance of heterogeneous perimeter control. This creates a need for a metric with *intermediate spatial granularity* that accounts for the gap between the intersection-level and network-level metrics to effectively address the heterogeneous nature of perimeter control. To address this need, we provide a generalized notion of multi-hop pressure to provide a “deeper” inspection lens on the internal region congestion from the perspective of each perimeter intersection.

Empirically, we demonstrate that our heterogeneous control methodology based on leveraging multi-hop pressure to redistribute the total permitted inflow reduces collective travel time in comparison to the homogeneous approach and the special case of 1-hop pressure under imbalanced protected region congestion as shown in Figure 1.

Objective: The primary objective of this work is to generalize the existing myopic 1-hop traffic pressure metric to a *multi-hop* traffic pressure metric. Informed by the multi-hop pressure, a heterogeneous perimeter controller is expected to redistribute the total permitted inflow according to each feeder link’s specific condition aggregated by multi-hop traffic pressure.

Contributions:

1. We generalize the definition of traffic pressure to multi-hop downstream links. This generalization allows us to adjust how far we can reach downstream links, providing a customizable spatial granularity of metrics that bridges the gap between the overly extensive scope of MFDs and the very limited scope of the traditional traffic pressure metric;
2. We conduct empirical evaluations with a simple controller leveraging multi-hop pressure for heterogeneous perimeter control under scenarios of various demand heterogeneity.
3. We perform sensitivity analysis that shows the robustness of our approach against the uncertainties in turning ratio estimations.

LITERATURE REVIEW

Perimeter control

Perimeter control manages inter-regional transfer flows by gating the feeder links of protected regions, ensuring that each region's vehicle count does not surpass a critical value that would negatively impact traffic efficiency. Urban traffic networks frequently become oversaturated during rush hour, necessitating perimeter control. The delineation of a congested area is called perimeter identification, which can be executed statically [11] or dynamically [12]. Once the perimeter is identified, perimeter control operates at the network level [4, 5, 13, 14, 15, 16] and is particularly effective in oversaturated situations where adaptive traffic signal control alone is insufficient [13].

The architecture of a perimeter controller is usually two-stage. At each control step, at the first stage, the macroscopic (and inherently homogeneous) perimeter controller obtains the optimal total permitted inflow for the protected region at the macroscopic level. At the second stage, the heterogeneous perimeter controller redistributes the total permitted inflow to each entry intersection on the perimeter based on feeder link attributes such as capacity, traffic conditions such as queue length, and control plan around that entry intersection. The total permitted inflow at the first stage comes from works that study upon abstracted traffic networks [17, 18, 19, 20, 21, 22, 23] and are driven by macroscopic simulation with network transmission model and the macroscopic fundamental diagrams. These works are beyond the scope of heterogeneous perimeter control, because abstracted traffic networks do not have topology and hence do not need the redistribution of total permitted inflow. Nevertheless, these homogeneous perimeter controllers at the first stage provide high-level guidance for heterogeneous perimeter control at the second stage.

Heterogeneous perimeter controllers have different types of redistribution policies: rule-based, optimization-based, and learning-based. Rule-based policy redistributes inflows proportionally to the feeder links' saturation flows [4, 5, 24, 25]. Optimization-based policy formulates total permitted inflow redistribution problem as a knapsack problem, which could integrate the low demand or spillback on the feeder links [26], balancing queues on feeder links [27, 6, 28], waiting times on feeder links [27], and the experienced delay on feeder links [6, 29, 30]. Learning-based policy [16] leverages graph neural networks for redistribution and enforces penalties for violating the total permitted inflow. However, most of these redistribution policies focus only on the feeder links without considering the downstream traffic conditions while perimeter control intrinsically requires a broader view of downstream traffic.

Macroscopic fundamental diagrams

At the *network level*, Macroscopic Fundamental Diagrams (MFDs) describe the relationship between traffic production and congestion levels for homogeneous urban networks, which were initially proposed by [31] and reintroduced by [1, 2, 3]. Experimental findings in Yokohama (Japan) show that MFDs work in practice [32]. MFDs are also widely used in numerous studies such as congestion pricing [33], and traveler information dissemination [34]. The most famous applications of MFDs are perimeter control, especially for controller design and quantifying traffic efficiency. For example, the design of the Proportional Integral (PI) controller requires MFDs to calibrate coefficients for proportional and integral terms as well as setpoints [4, 5, 35, 13, 6, 18, 36]. Similarly, analytical control approaches such as optimal control [37], model predictive control [38], and switching algorithm on top of a linear quadratic regulator [15] require MFDs. However, the accuracy of MFD-based controllers is dependent on the spatial heterogeneity of congestion distribution within the protected region; high heterogeneity (or low homogeneity) of spatial distribution in congestion adversely affects the MFD's reliability [7, 39, 34]. Apart from the heterogeneous congestion, the accuracy of MFDs can also deteriorate if the detectors are not ideally located [40]. Besides, [41] found that MFDs in urban and highway hybrid networks are scattered, and the traffic control plan affects MFDs. Despite various

applications guided by MFDs, as network-level metrics, MFDs are spatially too broad to describe the local traffic conditions around the feeder links.

1-hop traffic pressure

At the *intersection level*, traffic pressure quantifies the traffic statistic difference (such as vehicle count or density) between upstream and downstream links [42], which is inspired by works [8, 9, 10] that tackle resources reallocation in wireless communication networks. The application of traffic pressure mainly focuses the MaxPressure control policy which determines phase activation [43, 44, 45, 46, 47] or green time assignment [48, 49, 28, 50] for the next control period in a decentralized structure, and the MaxPressure control is incorporated in perimeter control strategies [28]. [49, 51] pointed out that phase activation is likely to produce a confusing ordering of phases that brings frustration to drivers, resulting in dangerous actions. Hence, a fixed [49] or variable [51] cycle time and fixed phase ordering are combined with the MaxPressure control along with the stability proof. [46] combines vehicle rerouting with MaxPressure to improve performance.

There are many variations of definition for 1-hop traffic pressure. The link lengths are taken into account [48] so that the pressure of a short link with queued vehicles is higher than the pressure of a longer link with the same number of queued vehicles, i.e., the queue density is used instead of the queue length in pressure calculation. Such definition of traffic pressure is leveraged in the reward design within deep reinforcement learning for signal control [52]. To prioritize some phases, the phase weights are proposed by [53, 54] in pressure definition, along with the dynamic estimation of turning ratios and saturated flows are also proposed to be adaptive to the traffic flows. To improve fairness in waiting time, [47] incorporates traffic delay into the pressure definition, with controllable relative importance between delay and queues. To avoid the practical difficulty in queue measurement, [50] proposed using travel times instead of queues to define the pressure, and are tested in both simulated and real traffic environments. However, all these pressure variations only use the nearest downstream links, while perimeter control requires knowledge of the traffic conditions beyond the 1-hop neighbor.

Gaps in the literature: In terms of spatial granularity, MFDs fail to capture detailed traffic dynamics, and the existing 1-hop traffic pressure definition only considers the immediate downstream links without extending its scope to further downstream conditions. While perimeter control inherently looks at traffic conditions at a greater spatial horizon, neither MFDs nor existing traffic pressure meets the requirement for heterogeneous perimeter control.

Novelty in our work: In this work, we propose the multi-hop pressure that has customizable spatial granularity to address the shortcomings of 1-hop pressure and MFDs. Informed by multi-hop pressure, we designed a simple yet efficient heterogeneous perimeter controller and tested scenarios with different levels of heterogeneity. Furthermore, sensitivity analyses are conducted to evaluate the robustness of the proposed controller.

PROBLEM STATEMENT

A perimeter control problem with a single protected region is formulated for its simplicity. In Figure 1a, the abstract traffic network consists of one protected region bounded by the perimeter, and there are several feeder links around the perimeter. A fixed control plan of traffic signals is used for intersections in the protected region. During high traffic demand periods, such as morning rush hour, incoming vehicles from feeder links are regulated to protect the region from being oversaturated. Only incoming vehicles are restricted, while outgoing vehicles are unaffected. At each control step, the controller sets the permitted inflow for each

metering device. Flow meterings are used instead of green timings for gating due to their simpler control nature, which eases the complexity of validation and implementation. The objective of perimeter control is to minimize the total time spent (TTS) for all the trips.

There are two types of perimeter control in terms of the action space: *homogeneous* perimeter control and *heterogeneous* perimeter control. Homogeneous perimeter control applies an identical permitted inflow rate to all feeder links regardless of the traffic condition. In contrast, heterogeneous perimeter control applies a permitted inflow rate dependent on each feeder link's traffic condition. Given the contrasting nature of these two types of perimeter control, we can make the following foundational assertions about their respective solution spaces:

- **Proposition 1:** The solution space of a homogeneous perimeter control is a subset of the solution space of a heterogeneous perimeter control.
- **Proposition 2:** There exists at least one solution in the solution space of the heterogeneous perimeter control, such that the performance of this solution is greater than (at least equal to) the performance of a homogeneous perimeter control.

Mathematical notations

The mathematical notations are primarily introduced in this section, where we establish the essential concepts. Notations related to specific methodologies or experimental setups are introduced in later sections to maintain relevance and coherence for better readability.

- a_t^i [veh/h] (**Control action**): the permitted inflow for metering device i at timestep t .
- a_{\min} [veh/h]: constant, lower bound of control action.
- a_{\max} [veh/h]: constant, upper bound of control action.
- N_F [unitless]: constant, the total number of controlled flow metering devices.
- \mathbf{a}_t [veh/h]: vectorized notation of control actions at timestep t . $\mathbf{a}_t = [a_t^1 \ \dots \ a_t^{N_F}]$.
- \bar{a}_t [veh/h]: the homogeneous action value set at timestep t for each metering device.
- $Q(l)$ [veh/km]: queue density of link l , which is the number of vehicles slower than 5km/h divided by the link length.
- Q_{\max} [veh/km/lane or veh/km/link]: constant, the maximal queue density when a lane or link is full. For a single lane $Q_{\max} = 209\text{veh/km/lane}$, which is reasonable for an average car length of 4m and an average bumper-to-bumper distance of 0.78m. For a 2-lane link, $Q_{\max} = 2 \times 209\text{veh/km}/(2 \times \text{lane}) = 418\text{veh/km/link}$.
- \mathcal{F} : the set of feeder links. The cardinality of the set is $|\mathcal{F}| = N_F$.
- \mathcal{V} : the set of the whole traffic network's links, i.e., all feeder links and all non-feeder links. This is also the set of vertices in graph representation.
- \mathcal{E} : the set of edges in graph representation. Each edge represents a permissible turning movement.
- Ω : supersink. See Definition 1.
- \mathcal{V}^e : the extended set of traffic links. The supersink is included compared to \mathcal{V} . See Definition 2.

- \mathcal{E}^e : the extended set of edges. See Definition 2.
- $G = (\mathcal{V}, \mathcal{E})$: the graph representation of the traffic network without supersink.
- $G^e = (\mathcal{V}^e, \mathcal{E}^e)$: the graph representation of the traffic network with supersink. See Definition 2.
- $\mathcal{N}(l, h)$: the set of h -hop downstream links from link l . 0-hop means the link itself, i.e., $\mathcal{N}(l, 0) = \{l\}$.
- $\Phi(l, h)$ [veh/km]: h -hop downstream potential for link l . See Definition 5.
- $p(l, h)$ [veh/km]: h -hop pressure for link l .
- T_{ij} [unitless]: turning ratio from link i to j . The summation of turning ratios from link i to all its 1-hop downstream links must be 1:

$$0 \leq T_{ij} \leq 1 \quad \forall i, j \quad (2)$$

$$\sum_{j \in \mathcal{N}(i, 1)} T_{ij} = 1 \quad \forall j \quad (3)$$

- $\mathbf{T} \in \mathbb{R}^{|\mathcal{V}| \times |\mathcal{V}|}$: the adjacency matrix of graph G where (i, j) -entry is T_{ij} .
- $\mathbf{P} \in \mathbb{R}^{|\mathcal{V}^e| \times |\mathcal{V}^e|}$: the adjacency matrix of graph G^e that can be constructed by extending matrix \mathbf{T} . \mathbf{P} is also a Markov transition matrix. See Eq. (9) for a full description.
- $\mathbf{Q} \in \mathbb{R}^{|\mathcal{V}^e|}$: the concatenation of queue density for links in set \mathcal{V}^e , where j^{th} entry is $\mathbf{Q}_j = Q(j)$. The arranging order of links must be the same as the row and column of \mathbf{P} .
- $\Phi(h) \in \mathbb{R}^{|\mathcal{V}^e|}$: the concatenation of h -hop downstream potential for links in set \mathcal{V}^e , where $\Phi_j(h) = \Phi(j, h)$. The arranging order of links must be the same as \mathbf{Q} .
- $\mathbf{p}(h) \in \mathbb{R}^{|\mathcal{V}^e|}$: the concatenation of h -hop pressure for links in set \mathcal{V}^e , where $\mathbf{p}_j(h) = p(j, h)$. The arranging order of links must be the same as \mathbf{Q} .

METHODOLOGY

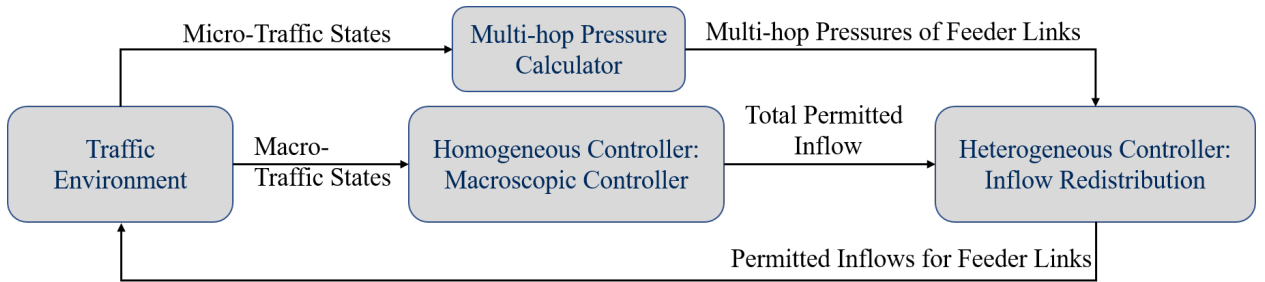


Figure 2 Two-stage control scheme: The first stage is a homogeneous controller that generates total permitted inflow. The second stage is a heterogeneous controller that redistributes the total permitted inflow as per multi-hop pressure at each feeder link.

The proposed perimeter control scheme is shown in Figure 2. The homogeneous controller computes the total permitted inflow at an aggregated level using macroscopic traffic states (e.g., traffic density of the region) from the traffic environment. Simultaneously, the multi-hop pressure calculator computes multi-hop pressures

of feeder links around the perimeter using microscopic traffic states (e.g., traffic density of each link). At the end of each control cycle, the total permitted inflow is redistributed by the heterogeneous controller, requiring the multi-hop pressures of feeder links.

The outline of this section is as follows: First, we present our graph-based representations of traffic networks, highlighting the incorporation of a “supersink” for destination aggregation to achieve the graph’s adjacency matrix to be a Markov chain transition matrix and reduce the size of the graph. Second, we propose the multi-hop pressure metric for evaluating traffic conditions over broader neighborhoods, and we provide mathematical formulations of pressure computation in the scalar form for a single link and the vectorized form for all links. Finally, this novel metric informs a heterogeneous controller based on the Softmax function to redistribute the total permitted inflow.

Traffic network modelling

We adopt a graph representation to represent the physical traffic network. To simplify the graph representation, we propose to merge all destinations with the concept of supersink. Another advantage of integrating the supersink is to achieve an adjacency matrix with the property of the Markov chain transition matrix, such that the interpretations of mathematical operations towards the adjacency matrix can be based on the Markov chain theory.

Supersink Ω : the merger of all destinations

Definition 1 (Supersink Ω). *A destination can be represented as a sink that absorbs vehicles. The supersink is considered as the merger of all destinations, and is the place where all trips finish. The prefix “super” refers to the abstracted meaning of sink without specifically indexing which destination the sink refers to. In contrast, the assignment of one non-super sink per destination is redundant for our purpose of building a Markovian adjacency matrix.*

There are three properties of the supersink: zero queue density, absorption, and binary turning ratio:

Property 1: Zero queue density The supersink does not reject vehicles from entering and has infinite storage capacity. Hence, the queue density of the supersink can be defined as 0:

$$Q(\Omega) = 0 \quad (4)$$

Property 2: Absorption The 1-hop neighbor of the supersink is still the supersink. Hence, any hop neighbor of the supersink is still the supersink:

$$\mathcal{N}(\Omega, h) = \{\Omega\}, \quad h \in \mathbb{N} \quad (5)$$

Before providing the third property of the supersink, we define an *exit link* in the traffic network to be a link that is *solely* connected to a destination. A real-world example of an exit link is a ramp to a parking lot. Mathematically, an exit link must satisfy:

$$\mathcal{N}(l, 1) = \{\Omega\} \quad (6)$$

Property 3: Binary turning ratio The turning ratio from the supersink to itself, and an exit link to the supersink are both 1, to other links is 0:

$$\begin{cases} T_{\Omega l} = 1 & \text{if } l = \Omega \\ T_{\Omega l} = 0 & \text{if } l \neq \Omega \end{cases} \quad (7)$$

$$\begin{cases} T_{l\Omega} = 1 & \text{if } \mathcal{N}(l, 1) = \{\Omega\} \\ T_{l\Omega} = 0 & \text{if } \mathcal{N}(l, 1) \neq \{\Omega\} \end{cases} \quad (8)$$

Graph representations of traffic networks

Definition 2 (Graph representation). The graph representation $G^e = (\mathcal{V}^e, \mathcal{E}^e)$, where:

- The extended link set $\mathcal{V}^e = \mathcal{V} \cup \{\Omega\}$ additionally includes a supersink vertex Ω .
- The extended edge set \mathcal{E}^e additionally includes those edges from exit links to the supersink, and the supersink to itself.
- Edge weight T_{uv} represents the turning ratio from link u to link v . These weights are derived from real empirical data or traffic simulations, encapsulating the probability of traffic flow transitions between links.

To provide an example of graph representation, a simplistic traffic network with 8 links, shown in Figure 3a, is mapped onto its graph representation depicted in Figure 3b.

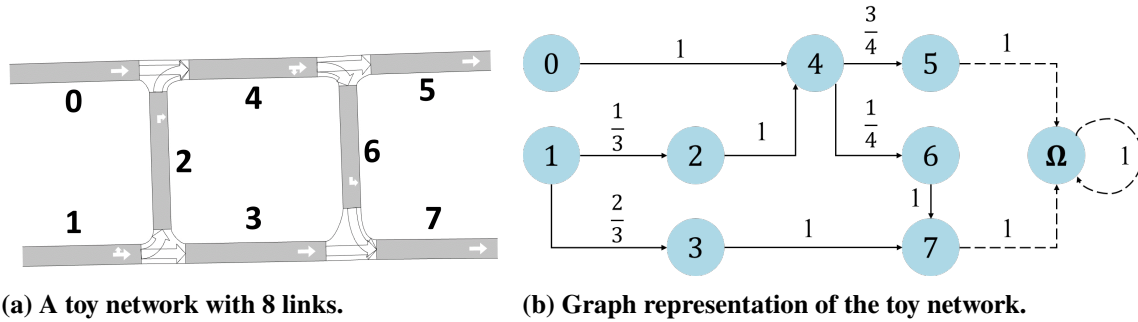


Figure 3 Toy network used for pressure calculation explanation. In Figure (a), there is no network beyond what is illustrated. In Figure (b), each vertex represents a traffic link, and each edge represents the connection of links, and the weights shown on the edges are the fabricated turning ratios. The vertex Ω is the supersink, and the edges in the dashed line represent graph G^e is extended from graph G .

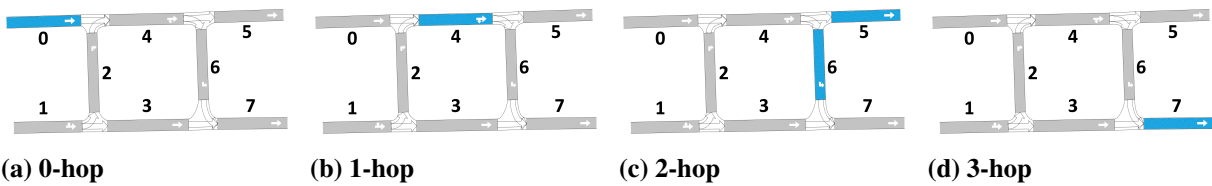


Figure 4 Link 0's downstream links (marked blue) at different hops.

A vehicle traveling in a traffic network according to certain turning ratios can be formalized as a time-homogeneous absorbing Markov chain by treating a vehicle presenting on a link l as a random variable

with probability $Pr(x = l)$. The state space of this Markov chain is a finite set with size $|\mathcal{V}^e|$. The transition matrix \mathbf{P} is exactly the adjacency matrix of graph \mathcal{G}^e , and is defined as follows:

$$\mathbf{P} = \begin{bmatrix} T_{11} & \dots & T_{1|\mathcal{V}|} & | & \mathbb{1}_1 \\ \vdots & \ddots & \vdots & | & \vdots \\ T_{|\mathcal{V}|1} & \dots & T_{|\mathcal{V}||\mathcal{V}|} & | & \mathbb{1}_{|\mathcal{V}|} \\ \hline 0 & \dots & 0 & | & 1 \end{bmatrix} = \begin{bmatrix} \mathbf{T} & \mathbb{1} \\ \mathbf{0}^\top & 1 \end{bmatrix}, \mathbb{1}_l = \begin{cases} 1 & \text{if } \mathcal{N}(l, 1) = \{\Omega\} \\ 0 & \text{if } \mathcal{N}(l, 1) \neq \{\Omega\} \end{cases} \quad (9)$$

Multi-hop pressure: a customizable metric for long-distance traffic condition

Congestion on a nearby street has a more immediate and significant impact than congestion several blocks away. Therefore, the multi-hop pressure definition needs to capture the diminishing influence of distant congestion while still accounting for its cumulative effect on the current traffic link. To understand the downstream links at different hops, Figure 4 illustrates the set of downstream links for link 0 at different hops. Mathematically, it is written as:

$$\mathcal{N}(0, 0) = \{0\} \quad (10)$$

$$\mathcal{N}(0, 1) = \{4\} \quad (11)$$

$$\mathcal{N}(0, 2) = \{5, 6\} \quad (12)$$

$$\mathcal{N}(0, 3) = \{7\} \quad (13)$$

$$\mathcal{N}(0, h) = \{\Omega\}, \quad h \geq 4, h \in \mathbb{N}^+ \quad (14)$$

In the following content, we first derive multi-hop pressure for a single link, and then we vectorize the scalar version to simultaneously compute the pressures of all links.

Scalar version: multi-hop pressure for a single link

To gently guide the reader step-by-step, we first review the standard 1-hop traffic pressure, then demonstrate how to extend the 1-hop traffic pressure to 2-hop and higher-hop versions.

1-hop Pressure: Adopted from physics, the existing standard 1-hop traffic pressure [44] is defined as the difference between upstream queue density and the summation of 1-hop downstream queue densities weighted by turning ratios. Mathematically, for a link l , its 1-hop pressure is:

$$p(l, 1) = Q(l) - \sum_{j \in \mathcal{N}(l, 1)} T_{lj} Q(j) \quad (15)$$

Apparently, 1-hop pressure is myopic in terms of knowing the traffic conditions further down the link of interest. When considering further neighborhoods, the concept of 1-hop pressure can be extended to multi-hop pressure to account for a wider range of traffic networks, capturing the cumulative effect of traffic congestion in neighboring areas.

2-hop Pressure: As per the requirement for multi-hop pressure, the congestion at 2-hop downstream links has less influence, and is naturally discounted by the turning ratio from link l to 1-hop downstream links:

$$p(l, 2) = Q(l) - \sum_{i_1 \in \mathcal{N}(l,1)} T_{li_1} \left(Q(i_1) + \sum_{i_2 \in \mathcal{N}(i_1,1)} T_{i_1 i_2} Q(i_2) \right) \quad (16)$$

$$= Q(l) - \underbrace{\sum_{i_1 \in \mathcal{N}(l,1)} T_{li_1} Q(i_1)}_{p(l,1)} - \sum_{i_1 \in \mathcal{N}(l,1)} \sum_{i_2 \in \mathcal{N}(i_1,1)} T_{li_1} T_{i_1 i_2} Q(i_2) \quad (17)$$

$$= p(l, 1) - \sum_{i_1 \in \mathcal{N}(l,1)} \sum_{i_2 \in \mathcal{N}(i_1,1)} T_{li_1} T_{i_1 i_2} Q(i_2) \quad (18)$$

3-hop Pressure: Similarly, the influence of congestion at 3-hop downstream links should diminish even more, hence it is discounted by both turning ratios at 1-hop and 2-hop downstream links:

$$p(l, 3) = Q(l) - \sum_{i_1 \in \mathcal{N}(l,1)} T_{li_1} \left[Q(i_1) + \sum_{i_2 \in \mathcal{N}(i_1,1)} T_{i_1 i_2} \left(Q(i_2) + \sum_{i_3 \in \mathcal{N}(i_2,1)} T_{i_2 i_3} Q(i_3) \right) \right] \quad (19)$$

$$= Q(l) - \underbrace{\sum_{i_1 \in \mathcal{N}(l,1)} T_{li_1} \left(Q(i_1) + \sum_{i_2 \in \mathcal{N}(i_1,1)} T_{i_1 i_2} Q(i_2) \right)}_{p(l,2)} \quad (20)$$

$$- \sum_{i_1 \in \mathcal{N}(l,1)} \sum_{i_2 \in \mathcal{N}(i_1,1)} \sum_{i_3 \in \mathcal{N}(i_2,1)} T_{li_1} T_{i_1 i_2} T_{i_2 i_3} Q(i_3) \\ = p(l, 2) - \sum_{i_1 \in \mathcal{N}(l,1)} \sum_{i_2 \in \mathcal{N}(i_1,1)} \sum_{i_3 \in \mathcal{N}(i_2,1)} T_{li_1} T_{i_1 i_2} T_{i_2 i_3} Q(i_3) \quad (21)$$

Multi-hop Pressure: As you may notice, there exists a recursive relationship between two consecutive hops of pressure. The second term represents the additional pressure exerted on link l due to congestion h hops away that was not accounted for in $(h - 1)$ -hop pressure. By subtracting the second term, we isolate the pressure that is specifically due to the h -hop congestion, distinguishing it from the cumulative pressure calculated up to $h - 1$ hops:

$$p(l, h) = p(l, h - 1) - \sum_{i_1 \in \mathcal{N}(l,1)} \sum_{i_2 \in \mathcal{N}(i_1,1)} \dots \sum_{i_h \in \mathcal{N}(i_{h-1},1)} T_{li_1} T_{i_1 i_2} \dots T_{i_{h-1} i_h} Q(i_h) \quad (22)$$

Explained in graph walk and Markov chain, the product of h turning ratios in the second term is the probability of graph walk with exactly h edges that lead from vertex l to vertex i_h , and this probability measures the h -step influence of h -hop downstream link i_h towards link l . The summation in the second term accumulates all the influence of h -hop downstream links upon traffic link l .

The properties of multi-hop pressure are 1) the pressure monotonously decreases as the hop increases, and 2) for h -hop pressure with normalized queue density, it has a bounded range of $[-h, 1]$. For the proof of bound, please refer to the Appendix.

The sum of products is lengthy. Fortunately, we can simplify the notation thanks to the power of the Markov transition matrix, which is detailed in the consequent section.

Vectorized version: multi-hop pressure for all links

Unlike the scalar version can only compute pressure for one link, the vectorized version can compute pressures for *all* links in the traffic network simultaneously. The vectorized form leverages the same recursive principle but in a compact, holistic manner. In addition, the vectorized form accelerates the computation upon implementation compared to iterating over each link in the network:

$$\mathbf{p}(0) = \mathbf{Q} \quad (23)$$

$$\mathbf{p}(h) = \mathbf{p}(h-1) - \mathbf{P}^h \mathbf{Q}, \quad h \in \mathbb{N}^+ \quad (\text{Recursive form}) \quad (24)$$

$$\mathbf{p}(h) = \mathbf{Q} - \sum_{h'=1}^h \mathbf{P}^{h'} \mathbf{Q}, \quad h \in \mathbb{N}^+ \quad (\text{Unrolled form}) \quad (25)$$

To make the recursive equation include $h = 1$ case, Eq. (23) defines the 0-hop pressure to be the queue density of the link. For the proof of the unrolled form in Eq. (25), please refer to the Appendix.

Interpretations of \mathbf{P}^h It is noteworthy to articulate the term \mathbf{P}^h in Eq. (24). Generally speaking, in the Markov chain, the entry (i, j) in the h -power of transition matrix \mathbf{P}^h , denoted as $(\mathbf{P}^h)_{ij}$, represents the probability of starting from vertex i and reaching vertex j after h steps of transitions. In the context of a traffic network where entries represent turning ratios, $(\mathbf{P}^h)_{ij}$ represents the probability of a vehicle moving from link i to link j considering all possible paths of h links.

h -hop influence: The scalar value $(\mathbf{P}^h)_{ij}$ captures the influence that the traffic state of link j has on link i after h transitions, that is, link j is one of the h -hop downstream links from link i , i.e., $j \in \mathcal{N}(i, h)$. It embodies the idea that traffic pressure is not local but can propagate through the network from distant links. This concept is formalized as *h -hop downstream link importance* in Definition 3.

Decay of influence over hop: Since \mathbf{P}^h involves higher powers of \mathbf{P} as h increases, the influence on pressure generally diminishes with hop due to the range of turning ratios being $[0, 1]$. This reflects the realistic attenuation of congestion effects over distance in a traffic network.

Pressure contribution: Multiplying $(\mathbf{P}^h)_{ij}$ by \mathbf{Q}_j incorporates the current traffic state (queue density) of link j into the pressure calculation at link i . If \mathbf{Q}_j is high (indicating congestion), and $(\mathbf{P}^h)_{ij}$ is significant, then link j will contribute substantially to the pressure at link i . The accumulation of $(\mathbf{P}^h)_{ij} \mathbf{Q}_j$ over all h -hop downstream links is formalized as *h -hop downstream potential* in Definition 5.

Equivalent definition of multi-hop pressure using potentials

Adopted from physics, another perspective for the pressure is the difference between upstream potential and downstream potential. Before defining potential, we first define *h -hop downstream link importance* and *downstream link accumulative importance*.

Definition 3 (*h -hop downstream link importance*). *The importance of a h -hop downstream link j to link l , noted as $w_{lj}(h)$, describes how the traffic condition on link j impacts upstream link l . We define the importance to be the probability of a vehicle released from link l being present on link j after traveling h links, which is exactly the (l, j) entry of \mathbf{P}^h :*

$$w_{lj}(h) = (\mathbf{P}^h)_{lj} \quad (26)$$

Such definition focuses on the importance of a specific hop. However, a vehicle can reach downstream link j in different hops by taking longer routes. In graph walk language, there may exist different lengths of paths from vertex l to j . Hence, to account for the impact of downstream link j from various hops, we need to accumulate the importance of each hop:

Definition 4 (Downstream link accumulative importance). *The accumulative importance of downstream link j for link l is a summation of 1-hop to h -hop downstream link importance:*

$$\hat{w}_{lj}(h) = \sum_{h'=1}^h w_{lj}(h') = \sum_{h'=1}^h (\mathbf{P}^{h'})_{lj} \quad (27)$$

Therefore, the accumulative importance combines the importance of downstream link j reached from different hops, unlike Definition 3 that only describes a specific length (hop).

Definition 5 (h -hop downstream potential). *Given a network graph $G^e = (\mathcal{V}^e, \mathcal{E}^e)$ of a traffic network, and a link l , its h -hop downstream potential $\Phi(l, h)$ is a sum over the queue density of link l 's h -hop downstream links weighted by the link importance:*

$$\Phi(l, h) = \sum_{j \in \mathcal{N}(l, h)} (\mathbf{P}^h)_{lj} \mathbf{Q}_j = (\mathbf{P}^h)_{l, :} \mathbf{Q}, \quad h \in \mathbb{N} \quad (\text{Scalar form}) \quad (28)$$

$$\Phi(h) = \mathbf{P}^h \mathbf{Q}, \quad h \in \mathbb{N} \quad (\text{Vectorized form}) \quad (29)$$

Following the introduction of potentials, the equivalent definition of h -hop pressure to Eq. (24) is the difference between 0-hop potential and cumulative downstream potentials from 1-hop to h -hop:

Definition 6 (h -hop pressure). *Given a graph $G^e = (\mathcal{V}^e, \mathcal{E}^e)$, and a link l , its h -hop pressure $p(l, h)$ is a difference between 0-hop downstream potential and cumulative higher-hop downstream potentials:*

$$p(l, h) = \Phi(l, 0) - \sum_{h'=1}^h \Phi(l, h'), \quad h \in \mathbb{N}^+ \quad (\text{Scalar form}) \quad (30)$$

$$\mathbf{p}(h) = \Phi(0) - \sum_{h'=1}^h \Phi(h'), \quad h \in \mathbb{N}^+ \quad (\text{Vectorized form}) \quad (31)$$

This equivalent multi-hop pressure definition factors in traffic states further downstream, giving a more comprehensive representation of the congestion and allowing for proactive adjustments.

Example: multi-hop pressure calculation on a simplistic traffic network

In this part, we provide an example of how to calculate multi-hop pressure for all links simultaneously.

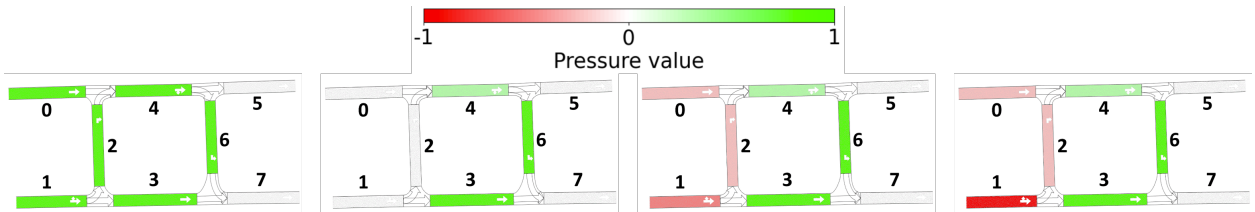


Figure 5 Visualization of each link's 0-hop, 1-hop, 2-hop, and 3-hop pressure (from left to right). Lower hops (0 and 1 hop) of pressures cannot distinguish links 0 and 1, but higher hops (at least 2 hops) can.

To compute the multi-hop pressure, first, we need to write down the adjacency matrix \mathbf{P} for the graph shown in Figure 3b, where the order arrangement of rows and columns corresponds to the link index in ascending order:

$$\mathbf{P} = \begin{bmatrix} 0 & 0 & 0 & 0 & 1 & 0 & 0 & 0 & 0 & 0 \\ 0 & 0 & \frac{1}{3} & \frac{2}{3} & 0 & 0 & 0 & 0 & 0 & 0 \\ 0 & 0 & 0 & 0 & 1 & 0 & 0 & 0 & 0 & 0 \\ 0 & 0 & 0 & 0 & 0 & 0 & 0 & 0 & 1 & 0 \\ 0 & 0 & 0 & 0 & 0 & \frac{3}{4} & \frac{1}{4} & 0 & 0 & 0 \\ 0 & 0 & 0 & 0 & 0 & 0 & 0 & 0 & 0 & 1 \\ 0 & 0 & 0 & 0 & 0 & 0 & 0 & 0 & 1 & 0 \\ 0 & 0 & 0 & 0 & 0 & 0 & 0 & 0 & 0 & 1 \\ 0 & 0 & 0 & 0 & 0 & 0 & 0 & 0 & 0 & 1 \end{bmatrix} \in \mathbb{R}^{9 \times 9} \quad (32)$$

Then, we define the vector of normalized queue densities \mathbf{Q} by assuming full congestion at links 0, 1, 2, 3, 4, and 6, while the other links do not have queued vehicles:

$$\mathbf{p}(0) = \mathbf{Q} = [1 \ 1 \ 1 \ 1 \ 1 \ 0 \ 1 \ 0 \ 0 \ 0]^\top \in \mathbb{R}^9 \quad (33)$$

To compute the multi-hop pressure for all links simultaneously, we leverage Eq. (24) to recursively calculate the pressure:

$$\mathbf{p}(1) = \mathbf{p}(0) - \mathbf{P}^1 \mathbf{Q} = [0 \ 0 \ 0 \ 1 \ \frac{3}{4} \ 0 \ 1 \ 0 \ 0 \ 0]^\top \in \mathbb{R}^9 \quad (34)$$

$$\mathbf{p}(2) = \mathbf{p}(1) - \mathbf{P}^2 \mathbf{Q} = [-\frac{1}{4} \ -\frac{1}{3} \ -\frac{1}{4} \ 1 \ \frac{3}{4} \ 0 \ 1 \ 0 \ 0 \ 0]^\top \in \mathbb{R}^9 \quad (35)$$

$$\mathbf{p}(3) = \mathbf{p}(2) - \mathbf{P}^3 \mathbf{Q} = [-\frac{1}{4} \ -\frac{5}{12} \ -\frac{1}{4} \ 1 \ \frac{3}{4} \ 0 \ 1 \ 0 \ 0 \ 0]^\top \in \mathbb{R}^9 \quad (36)$$

$$\mathbf{p}(h) = \mathbf{p}(3), \quad h \geq 3, h \in \mathbb{N} \quad (37)$$

The visualization of each link's 0-hop to 3-hop pressure is shown in Figure 5. Higher hops of pressure better distinguish link 0 and 1's downstream traffic conditions, whereas 0-hop and 1-hop pressure cannot differentiate them. Besides, as the number of hops increases, the pressure value decreases or remains the same depending on whether the downstream has queued vehicles.

Heterogeneous control: total permitted inflow redistribution leveraging multi-hop pressures

Once the multi-hop pressure is defined, the question leads to how can multi-hop pressure inform the design of heterogeneous controllers to redistribute the total permitted inflow. The controller must satisfy these two requirements:

1. **Monotonous increase relationship between pressure and control action:** a feeder link with larger pressure should be assigned with a larger permitted inflow rate since a larger pressure indicates more possibly unused capacities at downstream links.
2. **Total permitted inflow conservation:** The summation of all feeder links permitted inflows should equal to the total permitted inflow.

Following the requirements, we proposed the Softmax controller for its simplicity. We define *the perimeter h-hop pressure vector* $\mathbf{p}_t^F(h)$ to be the concatenation of h -hop pressure for each feeder link at timestep t :

$$\mathbf{p}_t^F(h) = \oplus_{f \in \mathcal{F}} p_t(f, h) \quad (38)$$

For feeder link $f \in \mathcal{F}$, its permitted inflow is:

$$a_t^f = (N_F \bar{a}_t) \times \text{Softmax}(s \mathbf{p}_t^F(h))_f \quad (39)$$

$$= (N_F \bar{a}_t) \times \frac{e^{s p_t(f, h)}}{\sum_{f \in \mathcal{F}} e^{s p_t(f, h)}} \quad (40)$$

where $(N_F \bar{a}_t)$ is the total permitted inflow at timestep t from the macroscopic (homogeneous) controller, and hyperparameter s is a positive scalar to tune the sensitivity to pressure values. When $s \rightarrow 0$, all permitted inflows are equal and the Softmax controller collapses into homogeneous control. When s is large, a feeder link with higher pressure is even more prioritized by greater permitted inflow. The choice of s is selected through experiments. Apparently, the summation of all feeder links' permitted inflows is the total permitted inflow owing to the property of the Softmax function. The action bound is set to $a_{\min} = 75 \text{ veh/h}$ and $a_{\max} = 3000 \text{ veh/h}$, respectively.

EXPERIMENTAL SETUP

The proposed perimeter control scheme is evaluated using the traffic simulator AIMSUN. Detailed description of the experimental setup in traffic network architecture and the traffic demand are provided in this section.

Traffic network architecture

As is shown in Figure 6, there are 24 feeder links around the perimeter and 36 signalized intersections with a fixed control plan in the protected region. Each traffic link is 85 meters long (each block is $2 \times 85 = 170$ meters long) with two lanes per link, except for links connected to an origin or destination have one lane only.

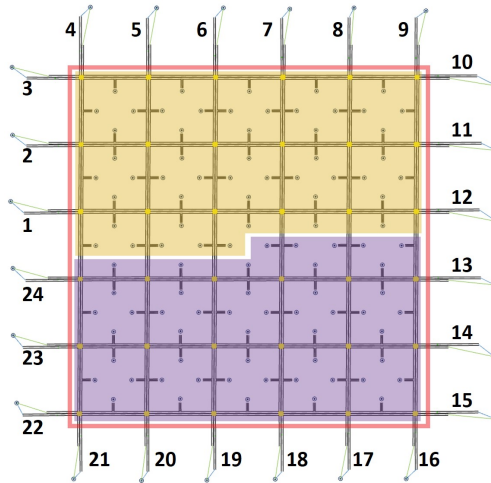


Figure 6 Tested traffic network. The protected region is bounded by a red rectangle as a perimeter, and the protected region is divided into two equal-sized upper and lower subregions, marked in yellow and purple, respectively. The subregions are for statistical purposes only, and there is no restriction of flow between subregions.

Heterogeneous demand setup

Does the performance improvement relative to homogeneous control increase as the demand heterogeneity increases? To answer this question, we design scenarios with different levels of demand heterogeneity. Our experiment examines two distinct approaches to modulating demand heterogeneity:

1. **Asynchrony:** the time difference between upper and lower subregions' demands. As asynchrony increases, we expect a rise in congestion heterogeneity.
2. **Imbalance:** the difference of demand volume generated in upper and lower subregions. As the imbalance increases, we expect a rise in congestion heterogeneity.

Below are necessary mathematical notations to describe the demand setup:

- T_S [hour]: the total traffic simulation duration.
- N_{12} [veh]: the total number of trips from feeder links to the protected region, i.e., external demand.
- N_{22} [veh]: the total number of trips from & to the protected region, i.e., internal demand.
- $D_{22}^{\text{upper}}(t)$ [veh/h]: the upper subregion internal demand at time t , each trip's origin and destination are in the upper subregion. The route of each trip may go beyond the upper subregion.
- $D_{22}^{\text{lower}}(t)$ [veh/h]: the lower subregion internal demand, each trip's origin and destination are in the lower subregion. The route of each trip may go beyond the lower subregion.
- $\alpha_{22}^{\text{upper}}$ [unitless]: the percentage of internal demand assigned to the upper subregion.
- $\alpha_{22}^{\text{lower}}$ [unitless]: the parameter of imbalance. The percentage of internal demand assigned to the lower subregion.
- $D_{12}^{\text{upper}}(t)$ [veh/h]: the demand profile for trips from upper feeder links (feeder link 1 to 12) to the upper subregion at time t . Trip origins are attached to upper feeder links, and destinations are in the upper subregion.
- $D_{12}^{\text{lower}}(t)$ [veh/h]: the demand profile for trips from lower feeder links (feeder link 13 to 24) to the lower subregion at time t . Trip origins are attached to lower feeder links, and destinations are in the lower subregion.
- τ [hour]: the parameter of asynchrony. The lateness (time shift) of demand profile $D_{12}^{\text{lower}}(t)$ and $D_{22}^{\text{lower}}(t)$ compared to demand $D_{12}^{\text{upper}}(t)$ and $D_{22}^{\text{upper}}(t)$.

The mathematical formulation of demand is as follows:

$$\int_0^{T_S} \left(D_{12}^{\text{lower}}(t) + D_{12}^{\text{upper}}(t) \right) dt = N_{12} \quad (41)$$

$$\int_0^{T_S} \left(D_{22}^{\text{lower}}(t) + D_{22}^{\text{upper}}(t) \right) dt = N_{22} \quad (42)$$

$$D_{12}^{\text{lower}}(t + \tau) = D_{12}^{\text{upper}}(t), \quad \forall t \quad (43)$$

$$\frac{D_{22}^{\text{lower}}(t + \tau)}{\alpha_{22}^{\text{lower}}} = \frac{D_{22}^{\text{upper}}(t)}{\alpha_{22}^{\text{upper}}}, \quad \forall t \quad (44)$$

$$\alpha_{22}^{\text{upper}} + \alpha_{22}^{\text{lower}} = 1 \quad (45)$$

$$0 < \alpha_{22}^{\text{upper}}, \alpha_{22}^{\text{lower}} < 1 \quad (46)$$

Eq. (41) and Eq. (42) indicate the total number of trips for external and internal demands. In this experiment, $N_{12} = 6000$ and $N_{22} = 11000$, respectively. Eq. (43) describes the asynchrony between demands from upper and lower feeder links. Eq. (44) describes the asynchrony and imbalance of internal demand. The asynchrony is regulated by the parameter τ , where a greater τ indicates later internal and external demands at the lower part of the traffic network. For imbalance, we adjust the parameter $\alpha_{22}^{\text{lower}}$ to vary the percentage of internal demand assigned to the lower subregion. $\alpha_{22}^{\text{lower}} = 50\%$ means equal volume of upper and lower subregion demands. As $|\alpha_{22}^{\text{lower}} - 50\%|$ increases, we expect a rise in congestion heterogeneity. Eq. (45) and Eq. (46) ensure the range for parameters related to imbalance. For simplification, there are no trips from the protected region to feeder links, or trips from feeder links to feeder links.

Tested demands The tested demands are designed based on the following questions:

1. How does the pressure sensitivity s affect the performance of the heterogeneous controller?
2. What is the range of hops such that the heterogeneous controller has the best performance?
3. Does the performance improvement increase as the demand heterogeneity increases for heterogeneous control?

For the first two questions, the heterogeneous demand is set with $\tau = \frac{3}{4}$ hour and $\alpha_{22}^{\text{upper}} = 50\%$. The sensitivity parameter s is tested with values of $2^0, 2^1, 2^2, 2^3, 2^4, 2^5, 2^6, 2^7$; the hop is tested with values of $0, 2, 4, \dots, 22$, and it is every 2 hops due to a vehicle requires to travel 2 links to cross each block in our traffic network. The maximal tested hop is 22 because the furthest downstream link is visited no more than 22 hops. Therefore, there are $8 \times 12 = 96$ combinations of s and hop.

For the third question, we test a range of τ and $\alpha_{22}^{\text{upper}}$ for the optimal controller selected from the best combination of s and hop in terms of minimal TTS. The value of τ is $0, \frac{1}{4}, \frac{2}{4}, \frac{3}{4}, 1$; and the value of $\alpha_{22}^{\text{upper}}$ is $50\%, 55\%, 60\%, 65\%, 70\%, 75\%, 80\%$. Therefore, there are $5 \times 7 = 35$ combinations of τ and $\alpha_{22}^{\text{upper}}$.

RESULTS & DISCUSSION

The results of the heterogeneous perimeter control with the Softmax controller are discussed in this section.

Control parameters and performance convergence: Figure 7 plots the TTS against varying levels of pressure sensitivity s for the Softmax controller, across different hops. The TTS is an average of simulations with 10 random seeds to address the traffic stochasticity. There is a clear trend of performance improvement compared to homogeneous control (labeled as 'homo') when the hop is increasing and converges after 10 hops. Moreover, an optimal range of pressure sensitivity s is identified between 2^3 and 2^4 , within which the Softmax controller achieves minimal TTS. Deviations outside this pressure sensitivity range, either too low or too high, would negatively affect the performance of the Softmax controller. Note that the optimal number of hops and pressure sensitivity are indicative of the tested traffic network and demands, while for other traffic networks and demands, the optimal hops and pressure sensitivity may need recalibration. The performance convergence after 10 hops provides a guideline for traffic sensor installation in a real-world implementation. Furthermore, the optimal range of pressure sensitivity emphasizes the calibration of control parameters.

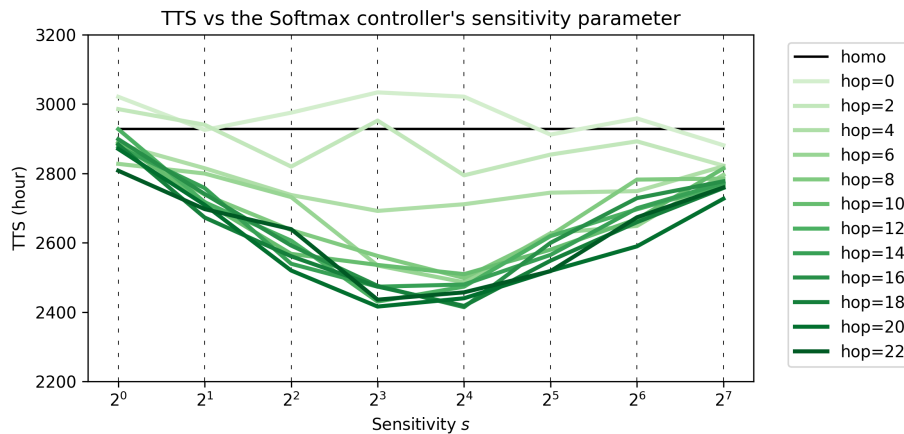


Figure 7 Performance vs. sensitivity for the heterogeneous controller.

Decayed impact of downstream links over hops: The performance convergence can be explained via Figure 8, which visualizes the 20-hop downstream link accumulative importance for feeder link 5. The accumulative importance reflects how traffic conditions from 1-hop to 20-hop downstream links impact the upstream traffic at feeder link 5. A darker color of a downstream link indicates a greater impact on feeder link 5. A distinct decay in importance with increasing hop is observed, emphasizing a trend where proximal downstream links exert a more pronounced effect on the feeder link than those distant downstream links. The decay pattern provides insight into the performance convergence beyond 10 hops: as the importance of downstream links diminishes over hop, the incremental contribution beyond 10 hops becomes increasingly negligible. This analysis validates the importance of downstream links in proximity and the rationale behind employing a finite spatial scope in multi-hop pressure.

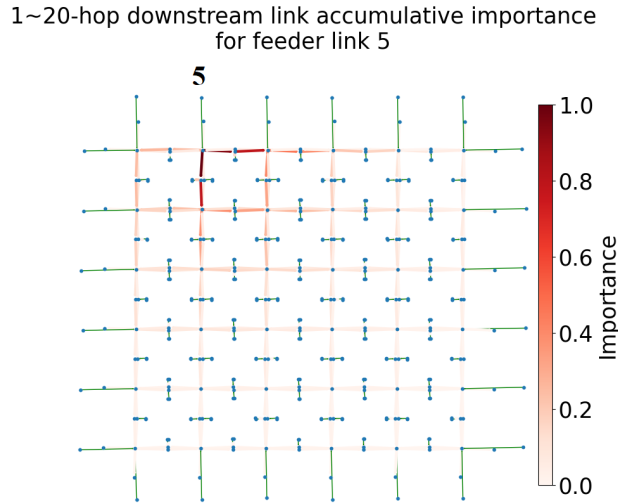


Figure 8 Heatmap of 20-hop downstream link accumulative importance for feeder link 5. The importance decays over hops, implying those near downstream links have a greater impact than those far downstream links.

Profile of pressures for each feeder link: In Figure 9, we compare the traffic pressure profiles under homogeneous control and heterogeneous control utilizing a Softmax controller. Both left and right figures capture the pressure at different hops for each feeder link at the same timestep. Under homogeneous control, the pressure profile on the left figure indicates a relatively imbalanced distribution across the feeder links, especially upper feeder links labeled in blue and lower feeder links labeled in red. This is because the homogeneous control cannot differentiate among the feeder links' varying congestion levels. The negative pressure with a large magnitude for lower feeder links indicates very congested downstream conditions. Conversely, the heterogeneous control demonstrates an equalized pressure distribution across feeder links. The small magnitude of pressures indicates the feeder link and its downstream have similar traffic potentials, and the downstream is not too congested. The Softmax controller modulates the total permitted inflow more adaptively by allocating higher permitted inflow to a feeder link with larger pressure (possibly an uncongested downstream) and reducing the permitted inflow to a feeder link with smaller pressure (possibly a congested downstream), potentially alleviating congestion in both feeder links and downstream.

Spectrum of downstream potentials: In Figure 10, we compare the spectrum of potential under homogeneous and heterogeneous controls at the same timestep. Under homogeneous control, the potential is larger than its heterogeneous control counterpart, which means the downstream congestion is more serious. Under either control, the potential generally decreases over time due to the decay of link importance. Besides, the

value of potential convergent towards zero aligns with the gradually flattened slope in the pressure profiles shown in Figure 9, as the difference of pressure is potential.

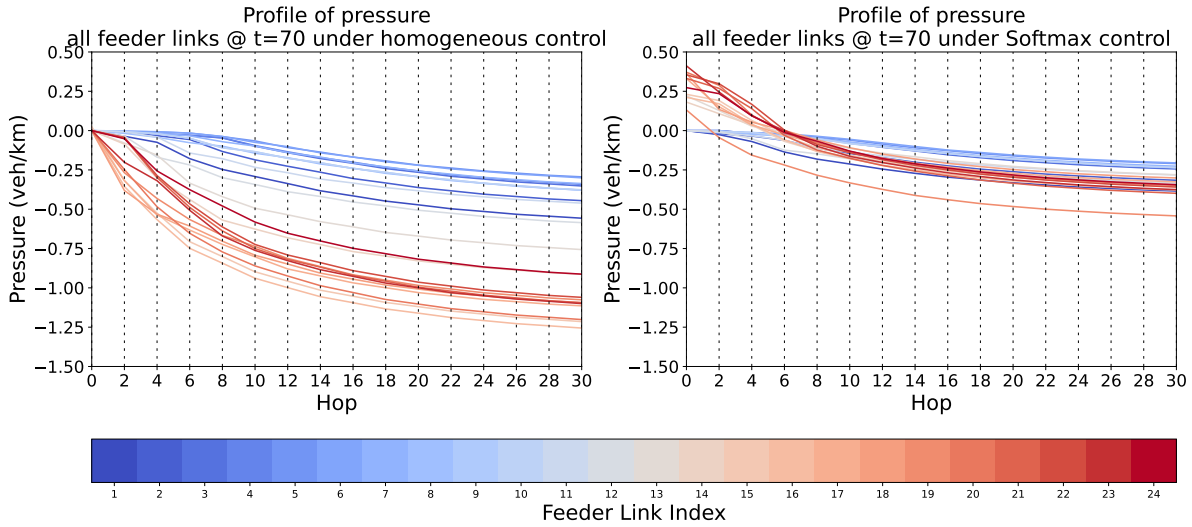


Figure 9 Profile of pressures for feeder links under homogeneous control and heterogeneous control. The heterogeneous control has more equalized (or balanced) pressure profiles than the homogeneous control; the heterogeneous control has smaller pressure profiles (in absolute value) than the homogeneous control.

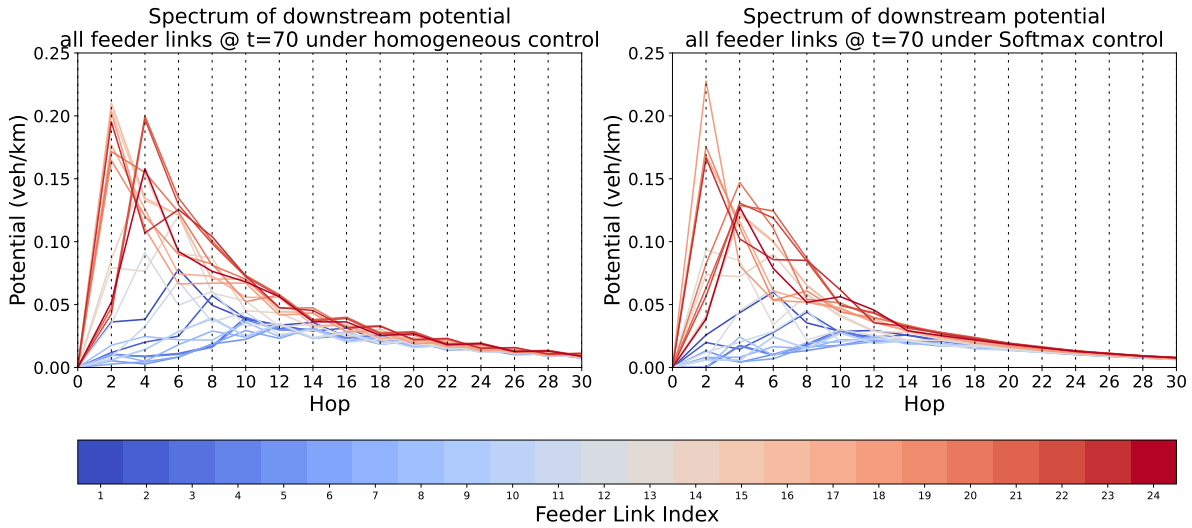


Figure 10 Spectrum of downstream potentials for feeder links under homogeneous control and heterogeneous control. The potentials are generally greater under homogeneous control compared to heterogeneous control, indicating a more congested downstream.

Performance improvement vs demand heterogeneity: Figure 11 shows a heatmap of how the performance improvement relates to two sources of demand heterogeneity: the demand shift τ and the upper subregion internal demand percentage $\alpha_{22}^{\text{upper}}$. The demand setup on the top right is the most heterogeneous, while the demand setup on the bottom left is the most homogeneous. The gradient of colors, ranging from green to red, conveys the magnitude of improvement, with more intense greens indicating higher performance improvement. Generally speaking, an increase in demand heterogeneity – represented by the configurations toward the top right of the heatmap – correlates with a more pronounced improvement in performance. Conversely, demand setup with lower heterogeneity, located around the bottom left of the heatmap, exhibits minimal or even negative performance improvement denoted by the light green and red cells. This trend demonstrates that the proposed heterogeneous controller is more effective in a more heterogeneous scenario.

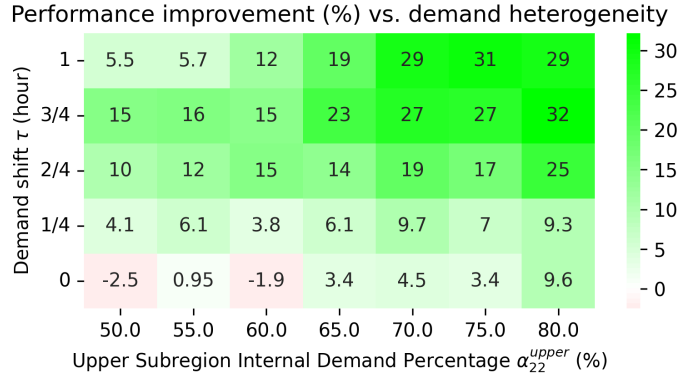


Figure 11 Performance improvement of the heterogeneous controller relative to the homogeneous control. Numbers in cells represent the performance improvement in percentage. The top right corner represents the most heterogeneous demand setup, while the bottom left corner represents the most homogeneous demand setup. The greater the demand heterogeneity, the better the performance of the heterogeneous controller.

SENSITIVITY ANALYSIS: ROBUSTNESS AGAINST TURNING RATIO PERTURBATIONS

Is the heterogeneous controller leveraging multi-hop pressure resilient to uncertainties in turning ratio estimations? The objective of this section is to assess the robustness of the multi-hop pressure-based approach when faced with turning ratio perturbations.

Experimental setup: The experimental design involves sampling turning ratios for each link in the traffic network. For each traffic simulation, the turning ratio of each link is sampled according to a probabilistic distribution and fixed during that simulation. The simulation is repeated 20 times for each distribution at a specified perturbation level to gather statistical data. To ensure the only random variable is the turning ratio, the simulation seed is fixed to 1.

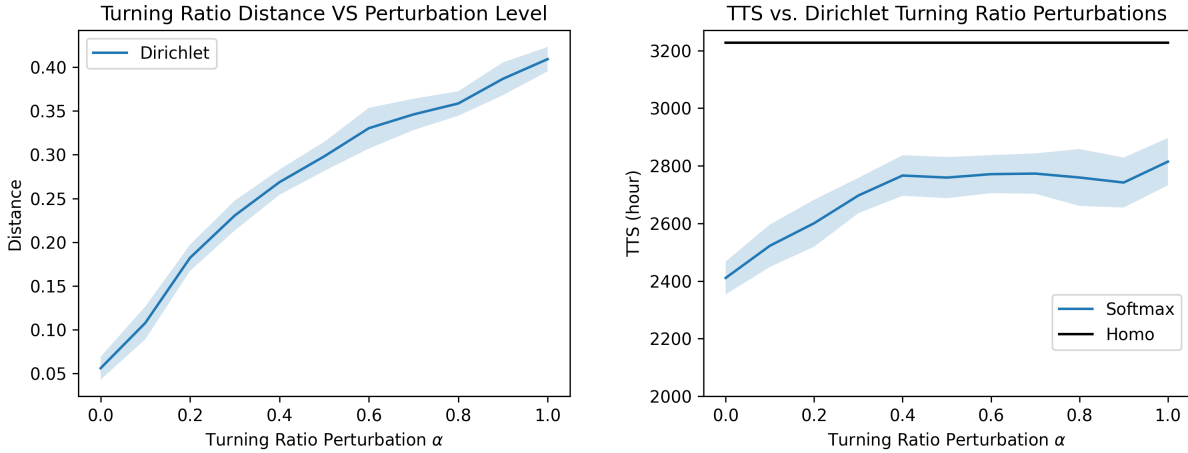
Turning ratio perturbations: The perturbed turning ratios are sampled from a Dirichlet distribution in which its sample naturally satisfies the property of probability space. The distribution is parameterized by a weighted average of the original turning ratios $\mathbf{T}_i = \sum_{j \in \mathcal{N}(i,1)} T_{ij}$ and a uniform vector $\mathbf{1}_i = \sum_{j \in \mathcal{N}(i,1)} \mathbf{1}$. The parameter $M = 100$ is the inverse temperature of the distribution:

$$\tilde{\mathbf{T}}_i \sim \text{Dir}(M(1 - \alpha)\mathbf{T}_i + M\alpha\mathbf{1}_i) \tag{47}$$

The degree of perturbation is controlled by the parameter $\alpha \in [0, 1]$, where $\alpha \rightarrow 0$ implies minimal perturbation and $\alpha \rightarrow 1$ signifies maximal perturbation. Notably, a setting of $\alpha = 1$ results in the expectation of equal turning ratios, e.g., $[\frac{1}{3}, \frac{1}{3}, \frac{1}{3}]$ for a link with three turning movements. To clarify, minimal perturbation ($\alpha = 0$) does not necessarily signify no perturbation. $\alpha = 0$ still results in a probabilistic distribution with non-zero entropy, and the mean of the distribution is the original turning ratio.

Turning ratio distance: To measure the discrepancy between the original and perturbed turning ratios, we define the turning ratio distance as a Euclidean distance:

$$d_i = \sqrt{(\tilde{\mathbf{T}}_i - \mathbf{T}_i)^\top (\tilde{\mathbf{T}}_i - \mathbf{T}_i)} \quad (48)$$



(a) Turn ratio distance vs. degree of perturbation α . (b) TTS vs. degree of perturbation α .

Figure 12 Robustness against turning ratio perturbations. (a) shows the turning ratio distance for an example of turning ratios $[0.56, 0.42, 0.02]$. A higher degree of perturbation leads to a larger turning ratio distance. (b) shows the performance under different levels of perturbation. A higher degree of perturbation leads to degraded performance, yet still outperforms homogeneous control.

Results: In this part, we show the result of the robustness of the heterogeneous controller against turning ratio perturbations. The robustness analysis against turning ratio perturbations reveals insightful trends in the Softmax controller’s performance. As expected, Figure 12a confirms a monotonic increase in the turning ratio distance with higher perturbation levels α . Notably, Figure 12b depicts performance degradation as perturbations intensify, emphasizing the controller’s sensitivity to turning ratio accuracy. Despite this, even at the highest perturbation level, where the mean of the Dirichlet distribution is equal turning ratios, the heterogeneous controller still outperforms the homogeneous control. It suggests that while the heterogeneous controller is affected by turning ratio perturbations, its adaptive mechanism still provides a superior alternative in managing traffic flow under uncertainty. Therefore, the result demonstrates the high robustness of our proposed approach.

CONCLUSION

This paper investigates the generalization of multi-hop traffic pressure for heterogeneous perimeter control. The multi-hop traffic pressure provides insight not only into immediate downstream link conditions but also

into the more distant traffic conditions. Our customizable long-distance traffic metric, grounded in Markov chain theory, bridges the gap between MFDs and 1-hop pressure where the spatial granularity is either too coarse or too fine. To account for the greater influence of closer traffic links, the multi-hop pressure naturally discounts distant downstream links by the product of turning ratios, interpreted as the multi-step transition probability in the Markov chain. This novel metric, supported by clean mathematical formulation, effectively guides heterogeneous perimeter control. A sensitivity analysis of the heterogeneous perimeter controller based on multi-hop pressure against turning ratio perturbation is conducted.

Analysis of results provides insights into the multi-hop pressure based on the heterogeneous controller. Within the optimal range of pressure sensitivity, the controller performs better than when the pressure sensitivity is beyond the optimal range, which emphasizes the calibration of control parameters. Besides, the performance convergence over hops indicates that knowing extremely distant traffic conditions does not contribute to performance improvement. Such convergence can be explained by the decay of downstream link importance over large hops. It provides a guideline for traffic sensor installation in field implementation. Furthermore, our result shows that performance improvement is greater when the demand heterogeneity is larger, whereas under the most homogeneous demand, the improvement is minimal. In addition, to evaluate the robustness of the heterogeneous controller, the sensitivity analysis involves experiments with different levels of perturbation toward turning ratios, and the result demonstrates strong robustness for the heterogeneous controller.

Future works could further 1) generalize the pressure definition by extending the upstream potential to multiple hops, 2) incorporate dynamic turning ratio estimation in multi-pressure calculation, 3) formulate other heterogeneous perimeter controllers, 4) test on a more complex city network, and 5) extend the application of multi-hop pressure to other traffic-related problems such as perimeter identification, congestion pricing, and adaptive traffic signal control.

Declaration of generative AI and AI-assisted technologies in the writing process: During the preparation of this work the authors used ChatGPT in order to improve the language and readability. After using this tool/service, the authors reviewed and edited the content as needed and take full responsibility for the content of the publication.

REFERENCES

- [1] Daganzo CF. Urban gridlock: Macroscopic modeling and mitigation approaches. *Transportation Research Part B: Methodological*. 2007;41(1):49–62.
- [2] Daganzo CF, Geroliminis N. An analytical approximation for the macroscopic fundamental diagram of urban traffic. *Transportation Research Part B: Methodological*. 2008;42(9):771–781.
- [3] Daganzo CF, Gayah VV, Gonzales EJ. Macroscopic relations of urban traffic variables: Bifurcations, multivaluedness and instability. *Transportation Research Part B: Methodological*. 2011;45(1):278–288.
- [4] Keyvan-Ekbatani M, Kouvelas A, Papamichail I, Papageorgiou M. Exploiting the fundamental diagram of urban networks for feedback-based gating. *Transportation Research Part B: Methodological*. 2012;46(10):1393–1403.
- [5] Keyvan-Ekbatani M, Papageorgiou M, Knoop VL. Controller design for gating traffic control in presence of time-delay in urban road networks. *Transportation Research Procedia*. 2015;7:651–668.
- [6] Keyvan-Ekbatani M, Carlson RC, Knoop VL, Papageorgiou M. Optimizing distribution of metered traffic flow in perimeter control: Queue and delay balancing approaches. *Control Engineering Practice*. 2021;110:104762.

- [7] Mazlounian A, Geroliminis N, Helbing D. The spatial variability of vehicle densities as determinant of urban network capacity. *Philosophical Transactions of the Royal Society A: Mathematical, Physical and Engineering Sciences*. 2010;368(1928):4627–4647.
- [8] Tassiulas L, Ephremides A. Stability properties of constrained queueing systems and scheduling policies for maximum throughput in multihop radio networks. In: *29th IEEE Conference on Decision and Control*. IEEE; 1990. p. 2130–2132.
- [9] Neely MJ, Modiano E, Rohrs CE. Dynamic power allocation and routing for time varying wireless networks. In: *IEEE INFOCOM 2003. Twenty-second Annual Joint Conference of the IEEE Computer and Communications Societies (IEEE Cat. No. 03CH37428)*. vol. 1. IEEE; 2003. p. 745–755.
- [10] Georgiadis L, Neely MJ, Tassiulas L, et al. Resource allocation and cross-layer control in wireless networks. *Foundations and Trends® in Networking*. 2006;1(1):1–144.
- [11] Saeedmanesh M, Geroliminis N. Clustering of heterogeneous networks with directional flows based on “Snake” similarities. *Transportation Research Part B: Methodological*. 2016;91:250–269.
- [12] Saeedmanesh M, Geroliminis N. Dynamic clustering and propagation of congestion in heterogeneously congested urban traffic networks. *Transportation research procedia*. 2017;23:962–979.
- [13] Keyvan-Ekbatani M, Gao X, Gayah VV, Knoop VL. Traffic-responsive signals combined with perimeter control: investigating the benefits. *Transportmetrica B: Transport Dynamics*. 2019;7(1):1402–1425.
- [14] Ren Y, Hou Z, Sirmatel II, Geroliminis N. Data driven model free adaptive iterative learning perimeter control for large-scale urban road networks. *Transportation Research Part C: Emerging Technologies*. 2020;115:102618.
- [15] Li Y, Mohajerpoor R, Ramezani M. Perimeter control with real-time location-varying cordon. *Transportation Research Part B: Methodological*. 2021;150:101–120.
- [16] Ni W, Cassidy MJ. Cordon control with spatially-varying metering rates: A Reinforcement Learning approach. *Transportation Research Part C: Emerging Technologies*. 2019;98:358–369. Available from: <https://www.sciencedirect.com/science/article/pii/S0968090X18312592>.
- [17] Haddad J, Geroliminis N. On the stability of traffic perimeter control in two-region urban cities. *Transportation Research Part B: Methodological*. 2012;46(9):1159–1176.
- [18] Haddad J, Shraiber A. Robust perimeter control design for an urban region. *Transportation Research Part B: Methodological*. 2014;68:315–332.
- [19] Geroliminis N, Haddad J, Ramezani M. Optimal Perimeter Control for Two Urban Regions With Macroscopic Fundamental Diagrams: A Model Predictive Approach. *IEEE Transactions on Intelligent Transportation Systems*. 2013;14(1):348–359.
- [20] Haddad J. Optimal perimeter control synthesis for two urban regions with aggregate boundary queue dynamics. *Transportation Research Part B: Methodological*. 2017;96:1–25. Available from: <https://www.sciencedirect.com/science/article/pii/S0191261516308025>.
- [21] Haddad J, Zheng Z. Adaptive perimeter control for multi-region accumulation-based models with state delays. *Transportation Research Part B: Methodological*. 2020;137:133–153.
- [22] Haddad J, Mirkin B. Resilient perimeter control of macroscopic fundamental diagram networks under cyberattacks. *Transportation research part B: methodological*. 2020;132:44–59.

- [23] Zhou D, Gayah VV. Model-free perimeter metering control for two-region urban networks using deep reinforcement learning. *Transportation Research Part C: Emerging Technologies*. 2021;124:102949. Available from: <https://www.sciencedirect.com/science/article/pii/S0968090X20308469>.
- [24] Aboudolas K, Geroliminis N. Perimeter and boundary flow control in multi-reservoir heterogeneous networks. *Transportation Research Part B: Methodological*. 2013;55:265–281. Available from: <https://www.sciencedirect.com/science/article/pii/S0191261513001185>.
- [25] Kouvelas A, Saeedmanesh M, Geroliminis N. Enhancing model-based feedback perimeter control with data-driven online adaptive optimization. *Transportation Research Part B: Methodological*. 2017;96:26–45.
- [26] Keyvan-Ekbatani M, Yildirimoglu M, Geroliminis N, Papageorgiou M. Multiple Concentric Gating Traffic Control in Large-Scale Urban Networks. *IEEE Transactions on Intelligent Transportation Systems*. 2015;16(4):2141–2154.
- [27] Papamichail I, Papageorgiou M. Balancing of queues or waiting times on metered dual-branch on-ramps. *IEEE Transactions on Intelligent Transportation Systems*. 2010;12(2):438–452.
- [28] Tsitsokas D, Kouvelas A, Geroliminis N. Two-layer adaptive signal control framework for large-scale dynamically-congested networks: Combining efficient Max Pressure with Perimeter Control. *Transportation Research Part C: Emerging Technologies*. 2023;152:104128.
- [29] Iordanidou GR, Papamichail I, Roncoli C, Papageorgiou M. Feedback-based integrated motorway traffic flow control with delay balancing. *IEEE Transactions on Intelligent Transportation Systems*. 2017;18(9):2319–2329.
- [30] Carlson RC, Ragias A, Papamichail I, Papageorgiou M. Mainstream traffic flow control of merging motorways using variable speed limits. In: 2011 19th Mediterranean Conference on Control & Automation (MED). IEEE; 2011. p. 674–681.
- [31] Godfrey J. The mechanism of a road network. *Traffic Engineering & Control*. 1969;8(8).
- [32] Geroliminis N, Daganzo CF. Existence of urban-scale macroscopic fundamental diagrams: Some experimental findings. *Transportation Research Part B: Methodological*. 2008;42(9):759–770.
- [33] Zheng N, Waraich RA, Axhausen KW, Geroliminis N. A dynamic cordon pricing scheme combining the macroscopic fundamental diagram and an agent-based traffic model. *Transportation Research Part A: Policy and Practice*. 2012;46(8):1291–1303.
- [34] Mahmassani HS, Saberi M, Zockaie A. Urban network gridlock: Theory, characteristics, and dynamics. *Procedia-Social and Behavioral Sciences*. 2013;80:79–98.
- [35] Keyvan-Ekbatani M, Carlson RC, Knoop VL, Hoogendoorn SP, Papageorgiou M. Queuing under perimeter control: Analysis and control strategy. In: 2016 IEEE 19th international conference on intelligent transportation systems (ITSC). IEEE; 2016. p. 1502–1507.
- [36] Ingole D, Mariotte G, Leclercq L. Perimeter gating control and citywide dynamic user equilibrium: A macroscopic modeling framework. *Transportation research part C: emerging technologies*. 2020;111:22–49.
- [37] Aalipour A, Kebriaei H, Ramezani M. Analytical optimal solution of perimeter traffic flow control based on MFD dynamics: a Pontryagin’s maximum principle approach. *IEEE Transactions on Intelligent Transportation Systems*. 2018;20(9):3224–3234.

- [38] Ramezani M, Haddad J, Geroliminis N. Dynamics of heterogeneity in urban networks: aggregated traffic modeling and hierarchical control. *Transportation Research Part B: Methodological*. 2015;74:1–19.
- [39] Geroliminis N, Sun J. Properties of a well-defined macroscopic fundamental diagram for urban traffic. *Transportation Research Part B: Methodological*. 2011;45(3):605–617.
- [40] Buisson C, Ladier C. Exploring the impact of homogeneity of traffic measurements on the existence of macroscopic fundamental diagrams. *Transportation Research Record*. 2009;2124(1):127–136.
- [41] Ji Y, Daamen W, Hoogendoorn S, Hoogendoorn-Lanser S, Qian X. Investigating the shape of the macroscopic fundamental diagram using simulation data. *Transportation Research Record*. 2010;2161(1):40–48.
- [42] Zhang R, Li Z, Feng C, Jiang S. Traffic routing guidance algorithm based on backpressure with a trade-off between user satisfaction and traffic load. In: *2012 IEEE Vehicular Technology Conference (VTC Fall)*. IEEE; 2012. p. 1–5.
- [43] Wongpiromsarn T, Uthaicharoenpong T, Wang Y, Frazzoli E, Wang D. Distributed traffic signal control for maximum network throughput. In: *2012 15th International IEEE Conference on Intelligent Transportation Systems*. IEEE; 2012. p. 588–595.
- [44] Varaiya P. Max pressure control of a network of signalized intersections. *Transportation Research Part C: Emerging Technologies*. 2013;36:177–195.
- [45] Varaiya P. The max-pressure controller for arbitrary networks of signalized intersections. In: *Advances in Dynamic Network Modeling in Complex Transportation Systems*. Springer; 2013. p. 27–66.
- [46] Zaidi AA, Kulcsár B, Wymeersch H. Traffic-adaptive signal control and vehicle routing using a decentralized back-pressure method. In: *2015 European Control Conference (ECC)*. IEEE; 2015. p. 3029–3034.
- [47] Wu J, Ghosal D, Zhang M, Chuah CN. Delay-based traffic signal control for throughput optimality and fairness at an isolated intersection. *IEEE Transactions on Vehicular Technology*. 2017;67(2):896–909.
- [48] Kouvelas A, Lioris J, Fayazi SA, Varaiya P. Maximum pressure controller for stabilizing queues in signalized arterial networks. *Transportation Research Record*. 2014;2421(1):133–141.
- [49] Le T, Kovács P, Walton N, Vu HL, Andrew LL, Hoogendoorn SS. Decentralized signal control for urban road networks. *Transportation Research Part C: Emerging Technologies*. 2015;58:431–450.
- [50] Mercader P, Uwayid W, Haddad J. Max-pressure traffic controller based on travel times: An experimental analysis. *Transportation Research Part C: Emerging Technologies*. 2020;110:275–290.
- [51] Levin MW, Hu J, Odell M. Max-pressure signal control with cyclical phase structure. *Transportation Research Part C: Emerging Technologies*. 2020;120:102828.
- [52] Wei H, Chen C, Zheng G, Wu K, Gayah V, Xu K, et al. Presslight: Learning max pressure control to coordinate traffic signals in arterial network. In: *Proceedings of the 25th ACM SIGKDD International Conference on Knowledge Discovery & Data Mining*; 2019. p. 1290–1298.
- [53] Xiao N, Frazzoli E, Li Y, Luo Y, Wang Y, Wang D. Further study on extended back-pressure traffic signal control algorithm. In: *2015 54th IEEE Conference on Decision and Control (CDC)*. IEEE; 2015. p. 2169–2174.

- [54] Xiao N, Frazzoli E, Luo Y, Li Y, Wang Y, Wang D. Throughput optimality of extended back-pressure traffic signal control algorithm. In: 2015 23rd Mediterranean Conference on Control and Automation (MED). IEEE; 2015. p. 1059–1064.

APPENDIX

Property of multi-hop pressure

1. Monotonously decreasing over the hop:

$$p(l, h) \leq p(l, h - 1) \quad (49)$$

2. Bounded range:

$$p(l, h) \in [-hQ_{\max}, Q_{\max}] \quad (50)$$

The upper bound is reached when the link itself is full and all its downstream links do not have queued vehicles. In contrast, the lower bound is reached when the link itself does not have queued vehicles and all its downstream are full of queued vehicles.

If we normalize queue density $Q(j)$ to $[0, 1]$ by dividing Q_{\max} , then

$$p(l, h) \in [-h, 1] \quad (51)$$

Proposition: Lower bound of h -hop pressure is $-h$:

Proof. By induction on h . Using the fact that the range of normalized queue density is $0 \leq Q(l) \leq 1$, for $h = 1$, we have

$$p(l, 1) = Q(l) - \sum_{j \in \mathcal{N}(l, 1)} T_{ij} Q(j) \geq 0 - \sum_{j \in \mathcal{N}(l, 1)} T_{ij} \times 1 = -1$$

Now assume the statement is true for some $h - 1$. Then

$$\begin{aligned} p(l, h) &= p(l, h - 1) - \sum_{i_1 \in \mathcal{N}(l, 1)} \sum_{i_2 \in \mathcal{N}(i_1, 1)} \dots \sum_{i_h \in \mathcal{N}(i_{h-1}, 1)} T_{li_1} T_{i_1 i_2} \dots T_{i_{h-1} i_h} Q(i_h) \\ &\geq -(h - 1) - \sum_{i_1 \in \mathcal{N}(l, 1)} \sum_{i_2 \in \mathcal{N}(i_1, 1)} \dots \sum_{i_h \in \mathcal{N}(i_{h-1}, 1)} T_{li_1} T_{i_1 i_2} \dots T_{i_{h-1} i_h} \times 1 \\ &= -(h - 1) - \sum_{i_1 \in \mathcal{N}(l, 1)} T_{li_1} \sum_{i_2 \in \mathcal{N}(i_1, 1)} T_{i_1 i_2} \dots \sum_{i_h \in \mathcal{N}(i_{h-1}, 1)} T_{i_{h-1} i_h} \\ &= -(h - 1) - 1 \times 1 \dots \times 1 \\ &= -(h - 1) - 1 \\ &= -h \end{aligned}$$

This proves the statement is also true for h . The claim is followed by mathematical induction. \square

Unrolled vectorized form of multi-hop pressure

We can unroll the recursive equation by plugging in the definition recursively until 0-hop pressure is reached:

$$\mathbf{p}(h) = \mathbf{p}(h - 1) - \mathbf{T}^h \mathbf{Q} \quad (52)$$

$$= \mathbf{p}(h - 2) - \mathbf{T}^{h-1} \mathbf{Q} - \mathbf{T}^h \mathbf{Q} \quad (53)$$

$$\dots \quad (54)$$

$$= \mathbf{p}(0) - \mathbf{T}^1 \mathbf{Q} - \mathbf{T}^{h-1} \mathbf{Q} - \mathbf{T}^h \mathbf{Q} \quad (55)$$

$$= \mathbf{Q} - \sum_{i=1}^h \mathbf{T}^i \mathbf{Q} \quad (56)$$

Efficient implementation of multi-hop pressure calculation

Leveraging the recursive relationship between $(h - 1)$ -hop and h -hop potentials, $\Phi(h) = \mathbf{P}\Phi(h - 1)$, we can write

$$\begin{bmatrix} \mathbf{p}(h) \\ \Phi(h) \end{bmatrix} = \begin{bmatrix} \mathbf{I} & -\mathbf{P} \\ \mathbf{O} & \mathbf{P} \end{bmatrix} \begin{bmatrix} \mathbf{p}(h - 1) \\ \Phi(h - 1) \end{bmatrix}, \quad h \in \mathbb{N}^+ \quad (57)$$

$$\begin{bmatrix} \mathbf{p}(0) \\ \Phi(0) \end{bmatrix} = \begin{bmatrix} \mathbf{Q} \\ \mathbf{Q} \end{bmatrix} \quad (58)$$

Let $\tilde{\mathbf{p}}(h) = \begin{bmatrix} \mathbf{p}(h) \\ \Phi(h) \end{bmatrix} \in \mathbb{R}^{2|\mathcal{V}^e|}$, $\mathbf{M} = \begin{bmatrix} \mathbf{I} & -\mathbf{P} \\ \mathbf{O} & \mathbf{P} \end{bmatrix} \in \mathbb{R}^{2|\mathcal{V}^e| \times 2|\mathcal{V}^e|}$, then

$$\tilde{\mathbf{p}}(h) = \mathbf{M}\tilde{\mathbf{p}}(h - 1), \quad h \in \mathbb{N}^+ \quad (59)$$

$$\tilde{\mathbf{p}}(0) = \begin{bmatrix} \mathbf{Q} \\ \mathbf{Q} \end{bmatrix} \quad (60)$$